20-μm slit expose the film for about one minute. Develop the film and, using one of the two methods described in Appendix D to determine unknown wavelengths, determine the wavelengths of the spectral lines.

You should first identify which $v' \rightarrow v''$ transition corresponds to which band. You will find reference 3 helpful in this identification.

For both the $C^3\Pi_u$ state and the $B^3\Pi_g$ state determine the rotational constants, $\bar{B}'_v$ and $\bar{B}''_v$, and the vibrational constants, ω'_e, x'_e, ω''_e, and x''_e, and then calculate the following:

1. The average internuclear separation
2. The vibrational energies
3. Dissociation energy
4. The Morse potential
5. Force constant k

Also calculate $h\nu_e$, the difference in electronic energy of the two states. Draw the Morse potential for both states and indicate the vibrational energies.

14. ZEEMAN EFFECT: OPTICAL SPECTROSCOPY

Historical Note

The 1902 Nobel prize in Physics was awarded jointly to
Hendrik Antoon Lorentz, the Netherlands, and Pieter Zeeman, the Netherlands
In recognition of the extraordinary service they rendered by their researches into the influence of magnetism upon radiation phenomena.

APPARATUS [Optional Equipment in Brackets]

^{198}Hg, Na, or He discharge lamp (preferably a Geissler tube)
Laboratory electromagnet [with tapered pole pieces]
Polarizer
Two converging lenses
Ebert spectrograph with photographic plates **or** Fabry–Perot etalon (mounted in vacuum can)
Constant-deviation prism spectrometer
Photomultiplier
Electrometer
Chart recorder

OBJECTIVES

To observe the Zeeman components for one or more spectral lines, measure the splittings, and compare the results with the predictions of theory.

To understand the physical origin of the Zeeman effect.

To be able to predict, for the case of weak external field and *LS* coupling, the number, relative intensities, polarizations, and splittings of the various components of a Zeeman multiplet.

KEY CONCEPTS

Multiplet	Zeeman energy
LS coupling	Polarization
Magnetic moment	*g* factor
Bohr magneton	Hamiltonian
Selection rules	Dipole matrix element
Fabry–Perot spectroscopy	Free spectral range
Finesse	Chromatic resolution

REFERENCES

1. R. Eisberg and R. Resnick, *Quantum Physics of Atoms, Molecules, Solids, Nuclei and Particles*, 2d ed., Wiley, New York, 1985. *LS* coupling and Zeeman effect are discussed in Chapter 10. Magnetic moments, the spin–orbit interaction, and transition matrix elements are treated in Chapter 8.
2. M. Nayfeh and M. Brussel, *Electricity and Magnetism*, Wiley, New York, 1985. Section 8.8 treats magnetic moments and orientational potential energy; the dipole radiation field is discussed in Chapter 15.
3. C. Candler, *Atomic Spectra*, 2d ed., Van Nostrand, Princeton, NJ, 1964. Chapters 6 and 16 treat the spectral line intensity rules for the Zeeman effect.
4. E. U. Condon and G. H. Shortley, *The Theory of Atomic Spectra*, Cambridge University Press, Cambridge, England, 1959. Quantum mechanical discussion of the Landé *g* factor (Chapter V) and of the spectral intensities (Chapter XVI). A classic reference.
5. B. Cagnac and J.-C. Pebay-Peyroula, *Modern Atomic Physics: Fundamental Principles*, Wiley, New York, 1975. Chapter 8 contains a development of the classical theory of the Zeeman effect that accounts for the observed polarizations.
6. E. Hecht, *Optics*, 2d ed., Addison-Wesley, Reading, MA, 1987. Section 9.6 discusses multiple beam interference devices, the Fabry–Perot interferometer in particular. Constant-deviation prisms are discussed briefly in Section 5.5.
7. G. Hernandez, *Fabry–Perot Interferometers*, Cambridge University Press, Cambridge, England, 1986. A detailed reference.
8. W. A. Hilton, *Am. J. Phys.* **30**, 724 (1962). Describes the construction and use of an inexpensive Fabry–Perot etalon.
9. S. Pollack and E. Wong, *Am. J. Phys.* **39**, 1387 (1971). Discusses light sources for the observation of the Zeeman effect. Since the writing of this article, Na Geissler tubes have become commercially available.
10. C. Manka and K. Mittelstaedt, *Am. J. Phys.* **41**, 287 (1973). Discusses the observation of the Zeeman effect for the 4046- and 5461-Å Hg lines using an Ebert spectrograph.
11. *Nobel Lectures: Physics*, Vol. 1, Elsevier, Amsterdam, 1967. On page 33 is a narrative account by Zeeman describing his investigations.

INTRODUCTION

When an atom makes a transition from an initial state to a final state of lower energy, a photon is emitted with an energy equal to the difference in energy of these states: A single spectral line is observed that corresponds to this transition. If either of the two states involved in the transition has a magnetic moment, then the application of an external

magnetic field **B** causes the spectral line to split into several closely spaced components, the extent of the splitting being proportional to B. In this experiment you will try to understand and observe this splitting, known as the Zeeman effect. In what follows, we first treat the relatively straightforward case of the Zeeman effect in "one-electron atoms" for large external magnetic fields; we then move to the more practical, but slightly more complex, case of small fields. Finally, we discuss the situation for multielectron atoms.

One-Electron Atoms

For many atoms, (e.g., Na) the optical spectrum is associated with transitions between states of a single electron outside a closed inner shell. This single *optically active* electron may have both an orbital and a spin magnetic moment. We can calculate the magnetic moment $\boldsymbol{\mu}_\ell$ associated with the orbital motion of this electron by use of a classical model in which it orbits in a circle of radius r with speed v, as in Figure 14.1*a*. The magnetic moment $\boldsymbol{\mu}$ is defined for any charge distribution as

$$\boldsymbol{\mu} \equiv \frac{1}{2}\int \mathbf{r} \times \mathbf{v}\, dq \qquad (\mathrm{C \cdot m^2/s}) \tag{1}$$

Evaluating this for an electron in a circular orbit, in terms of its angular momentum $\mathbf{L} \equiv \mathbf{r} \times m\mathbf{v}$, yields for $\boldsymbol{\mu}_\ell$

$$\boldsymbol{\mu}_\ell = -\frac{e}{2m}\mathbf{L} \qquad (\mathrm{C \cdot m^2/s}) \tag{2}$$

where the minus sign signifies that, for an electron, $\boldsymbol{\mu}_\ell$ is always opposed to **L**. This result is conventionally written in terms of g_ℓ, called the **orbital *g* factor**, and $\mu_0 \equiv e\hbar/2m$, called the **Bohr magneton**:

$$\boldsymbol{\mu}_\ell = -\frac{g_\ell \mu_0}{\hbar}\mathbf{L} \qquad (\mathrm{C \cdot m^2/s}) \tag{3}$$

where $g_\ell = 1$. If an external magnetic field **B** is applied, then, according to classical mechanics, $\boldsymbol{\mu}_\ell$ undergoes Larmor precession about **B** with angular frequency $\omega = g_\ell \mu_0 B/\hbar$, thus altering the motion of the electron, as discussed in reference 5. The total energy of the electron now depends on the relative orientation of $\boldsymbol{\mu}_\ell$ and **B** because the presence of the field contributes a magnetic (Zeeman) energy

$$E_Z^\ell = -\boldsymbol{\mu}_\ell \cdot \mathbf{B} \qquad (\mathrm{J}) \tag{4}$$

Different orientations of **L**, as depicted in Figure 14.1*b*, thus correspond to different values of E_Z^ℓ.

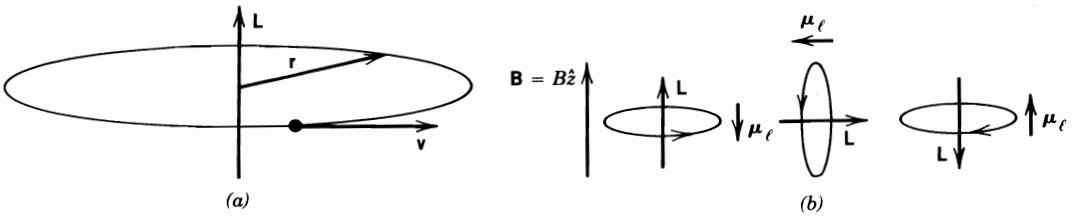

FIGURE 14.1 (*a*) Classical picture of an electron orbiting a nucleus. (*b*) Different orientations for the orbital angular momentum.

Since the electron also possesses a spin angular momentum **S**, there is an additional contribution to the magnetic moment of the atom, $\boldsymbol{\mu}_s$, given by analogy with equation 3 as

$$\boldsymbol{\mu}_s = -\frac{g_s \mu_0}{\hbar}\mathbf{S} \qquad (\mathrm{C \cdot m^2/s}) \tag{5}$$

with a corresponding contribution to the energy of

$$E_Z^s = -\boldsymbol{\mu}_s \cdot \mathbf{B} \qquad (\mathrm{J}) \tag{6}$$

The total magnetic (Zeeman) energy of the atom is thus

$$E_Z = -(\boldsymbol{\mu}_\ell + \boldsymbol{\mu}_s) \cdot \mathbf{B} \qquad (\mathrm{J}) \tag{7}$$

It must be noted that in the expression for $\boldsymbol{\mu}_s$, the **spin *g* factor** g_s is approximately 2, rather than 1, as for g_ℓ, a result of relativistic quantum mechanics. Precise spectroscopic measurements yield a value of $g_s = 2.00232$, as predicted by the more refined theory of quantum electrodynamics.

In the quantum-mechanical description of the one-electron atom, the state of the electron is described approximately, in the *absence* of any external **B**, by the wave function $\psi_{n,\ell,m_\ell,m_s}(r, \theta, \phi)$, which is an eigenfunction of the approximate Hamiltonian

$$H_0 = \frac{p^2}{2m} + V(r) \qquad (\mathrm{J}) \tag{8}$$

where V is the Coulomb potential energy of the electron, assumed spherically symmetric, and where we have ignored, for the moment, the spin–orbit interaction between the moving electron spin and the nucleus (discussed in Experiment 12 and briefly below). The four subscripts for ψ are the quantum numbers that describe the electron state. The positive integer n is the principal quantum number. The integer ℓ indexes the magnitude L of the orbital angular momentum **L** and can take on values from 0 through $n-1$; L is then given as $[\ell(\ell+1)]^{1/2}\hbar$. The integer m_ℓ ranges from $-\ell$ to $+\ell$ and indexes the z component (or the component along any fixed direction) of **L**:

$$L_z = m_\ell \hbar \qquad (\mathrm{J \cdot s}) \tag{9}$$

This number then specifies the orientation of the orbit mentioned above in connection with Figure 14.1*b*. The electron has a spin quantum number s which is not included in the subscript because it is always understood to be $\frac{1}{2}$; the magnitude of the spin angular momentum **S** is then given as $S = [s(s+1)]^{1/2}\hbar$ in analogy with L. The fourth quantum number m_s then gives the orientation of the spin (up or down) by specifying its z component:

$$S_z = m_s \hbar \qquad (\mathrm{J \cdot s}) \tag{10}$$

where m_s is either $+\frac{1}{2}$ or $-\frac{1}{2}$. The energy of the state corresponding to ψ now depends on n and ℓ but, since there is no magnetic field, is independent of m_ℓ and m_s, which determine the orientation of the moments $\boldsymbol{\mu}_\ell$ and $\boldsymbol{\mu}_s$.

We now go the high-field limit by applying a magnetic field along $\hat{z}$ that is so strong that the spin–orbit correction to the Hamiltonian H_0 of equation 8 is negligible by comparison with the Zeeman interaction. The Hamiltonian for the system is then approximated as $H \simeq H_0 + H_Z$, where H_Z is the Zeeman interaction Hamiltonian represented as the operator equivalent of equation 7. The energy E is now calculated using the time-independent

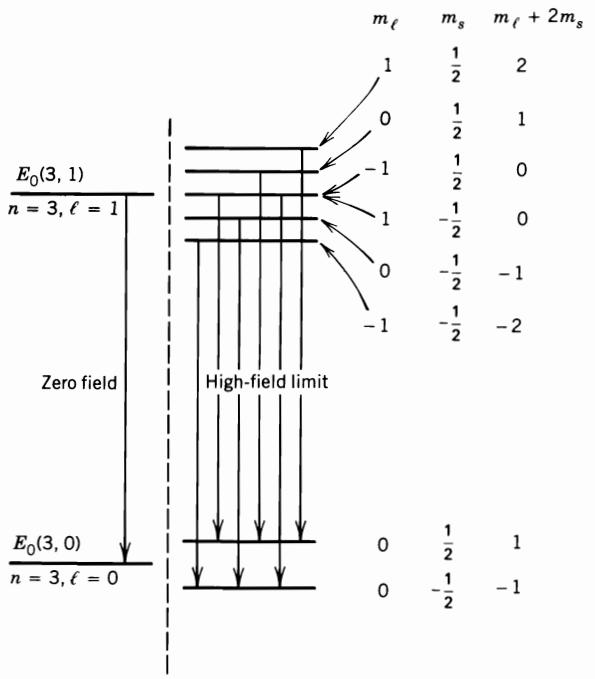

FIGURE 14.2 Effect of a very strong magnetic field on two atomic states.

Schrödinger equation, $H\psi = E\psi$, to give

$$E = E_0(n, \ell) + E_Z = E_0(n, \ell) + \mu_0 B(m_\ell + 2m_s) \qquad \text{(J)} \qquad (11)$$

where E_0 is the energy corresponding to H_0, the zero-field Hamiltonian, and the values $g_\ell = 1$ and $g_s = 2$ have been used. Figure 14.2 shows the effect of a very strong field on two states, one with $n = 3$, $\ell = 0$, and the other with $n = 3$, $\ell = 1$. Each of these levels, degenerate for $\mathbf{B} = 0$, splits in the presence of $\mathbf{B}$, as indicated to the right of the vertical dashed line; the extent of the splitting, since we have ignored the spin–orbit interaction, depends only on the sum $m_\ell + 2m_s$. Note that while only one transition (spectral line) is possible if $\mathbf{B} = 0$, the application of $\mathbf{B}$ produces a system of lines corresponding to the indicated transitions. For dipole radiation, only transitions obeying the selection rules $\Delta m_s = 0$, $\Delta m_\ell = 0, \pm 1$ are observed (the "allowed" transitions). These **selection rules** are based on the evaluation of the dipole matrix elements between initial and final states, and are discussed in Chapters 8 and 10 of reference 1.

EXERCISE 1

Estimate the energy splittings, in electron-volts, of the spectral lines corresponding to the transitions shown in Figure 14.2, as predicted by equation 11 for the high-field limit. Assume a magnetic field of $B \sim 10^6$ G (i.e., 10^2 T). What additional information would you need to determine the separation in wavelength for these lines?

Although the above calculation for the Zeeman splittings in the high-field limit is straightforward conceptually, magnetic fields appropriate to this limit are beyond the

capabilities of the electromagnets found in most undergraduate laboratories. In this experiment, the fields used are more appropriate to the weak-field limit, in which the effect of the spin–orbit interaction on the electronic states must be explicitly considered.

The spin–orbit interaction can be viewed as the interaction of the spin magnetic moment $\boldsymbol{\mu}_s$ of the electron with the internal magnetic field attributed to the motion of the positively charged nucleus as viewed in the rest frame of the orbiting electron. Since this internal field can be shown to be proportional to $\mathbf{L}$, the form of the interaction can be written as $H_{so} = \zeta(r)\mathbf{L} \cdot \mathbf{S}$, where $\zeta(r)$ is a function of the distance of the electron from the nucleus. The electron states in zero external field are now determined from a Hamiltonian $H' = H_0 + H_{so}$:

$$H' = \frac{p^2}{2m} + V(r) + \zeta(r)\mathbf{L} \cdot \mathbf{S} \qquad \text{(J)} \tag{8'}$$

The states ψ' are determined as eigenfunctions of H' with energies E', and the Zeeman energy E_Z, now assumed very small compared with the spin–orbit energy contribution E_{so}, is then calculated as a perturbation, using these states.

EXERCISE 2

The spin–orbit interaction may be written as $H_{so} = -\boldsymbol{\mu}_s \cdot \mathbf{B}_i$, where $\mathbf{B}_i$ represents the (spatially varying) internal magnetic field "seen" by the spinning electron due to its orbital motion with respect to the positively charged nucleus. Estimate the average magnitude of this internal field for an atom in which the average value of E_{so} is roughly 2×10^{-4} eV.

The states ψ' are different from the states ψ determined by H_0 above in that for the former, the angular momenta $\mathbf{L}$ and $\mathbf{S}$, although constant in *magnitude*, are no longer constant in *direction*: the $\mathbf{L} \cdot \mathbf{S}$ interaction causes them to precess about their sum, the *total* angular momentum $\mathbf{J} = \mathbf{L} + \mathbf{S}$, which is strictly constant. Thus, ℓ and s are still good quantum numbers, but m_ℓ and m_s are not; replacing these last two are j and m_j, which index the magnitude of $\mathbf{J}$ and its z component J_z, respectively. According to the quantum rules for the addition of angular momenta, j can assume any value from $|\ell - s|$ to $|\ell + s|$ in steps of 1, depending on the relative orientation of $\mathbf{L}$ and $\mathbf{S}$, as illustrated in Figure 14.3*a*. By analogy with these, the magnitude of $\mathbf{J}$ is given in terms of its index j as $J = [j(j+1)]^{1/2}\hbar$, while J_z is given in terms of m_j as

$$J_z = m_j\hbar \qquad \text{(J · s)} \tag{12}$$

Figure 14.3*b* shows the relationship between $\mathbf{J}$, $\mathbf{L}$, and $\mathbf{S}$ for an electron in the particular

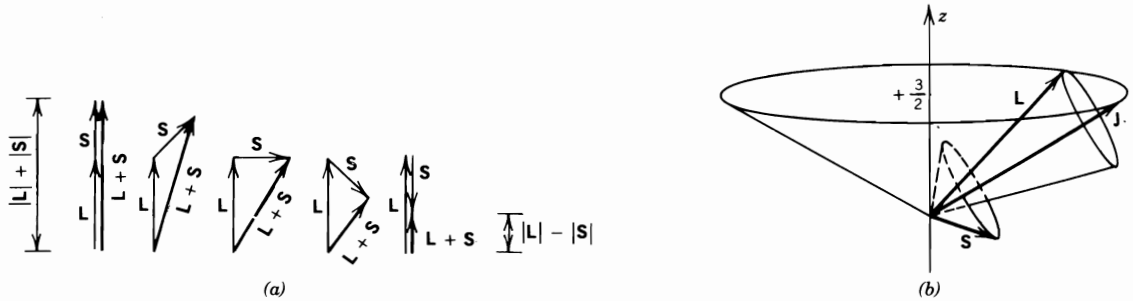

FIGURE 14.3 (*a*) Addition of angular momenta. (*b*) The relationship between $\mathbf{J}$, $\mathbf{L}$, and $\mathbf{S}$ for the case $\ell = 2, j = \frac{5}{2}, m_j = \frac{3}{2}$.

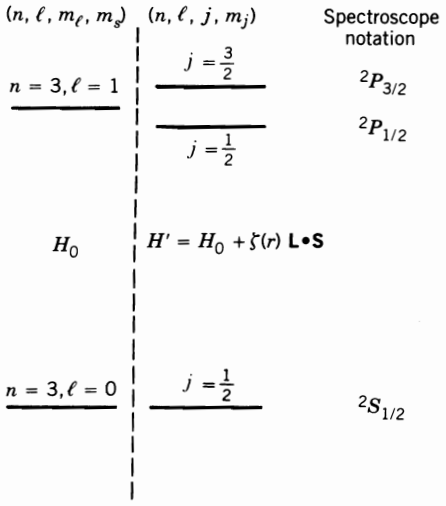

FIGURE 14.4 The effect of the spin–orbit interaction on $n = 3$ states.

case $\ell = 2$, $j = \frac{5}{2}$, $m_j = \frac{3}{2}$; note the vector **J** for this state is constant in time, but may lie anywhere in the cone for which $J_z = \frac{3}{2}\hbar$.

The states ψ' may thus be labeled as ψ'_{n,ℓ,j,m_j} and may be considered as arising from the states ψ_{n,ℓ,m_ℓ,m_s} when the $\mathbf{L}\cdot\mathbf{S}$ interaction is "turned on." This is depicted in Figure 14.4 for $n = 3$ states: The states (n, ℓ, m_ℓ, m_s), eigenfunctions of H_0, are drawn to the left of the vertical dashed line, while those of H' (n, ℓ, j, m_j) are to the right. Note that the $\ell = 1$ states are split into a *multiplet* of states, one for each value of j, by the spin–orbit interaction; the magnitude of the energy splitting is determined by the difference in the values of E_{so} calcuated for each state. States with different values of m_j, but the same value of j, have the same energy (are degenerate) in the absence of an external **B** field. The spectroscopic symbol to the right of each level is the conventional, compact notation used to specify the set of quantum numbers s, ℓ, j for each state in the form $^{2s+1}\ell_j$, where the capital letters correspond to different values of ℓ: $S = 0$, $P = 1$, $D = 2$, and so on.

EXERCISE 3

Verify that the coupling of ℓ and s for the states of H_0 in Figure 14.4 produces states with the j values indicated and that the spectroscopic notation is appropriate to each state of H'.

We can now calculate the Zeeman splittings of the levels characterized by the set of quantum numbers (n, ℓ, j, m_j) by evaluating E_Z of equation 7 for each of these states. This is a bit more difficult than for the high-field case, since $\boldsymbol{\mu}_\ell$ and $\boldsymbol{\mu}_s$, being proportional to **L** and **S**, respectively, are no longer constant in direction for these states. The calculation can be done by evaluating the matrix elements of the Zeeman Hamiltonian H_Z in operator form, but the vector model of the angular momenta discussed above provides an approach that is physically much more insightful.

Figure 14.5*a* shows how **L** and **S** (and, hence, $\boldsymbol{\mu}_\ell$ and $\boldsymbol{\mu}_s$) each precess about the constant vector **J** in the absence of an externally applied **B** field. The angular frequency of this precession is proportional to B_i, the strength of the internal field discussed in Exercise 2. If we now apply an external field **B** along the z direction that is much weaker than $\mathbf{B}_i$, then the precession of $\boldsymbol{\mu}_\ell$ and $\boldsymbol{\mu}_s$ about **J** is much more rapid than the precession of the total

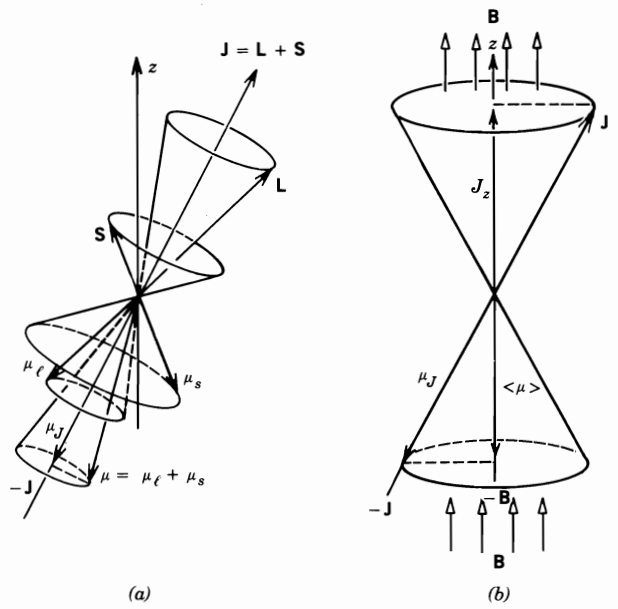

FIGURE 14.5 (*a*) **L** and **S** precessing about **J**. (*b*) **J** precessing about **B**.

moment $\boldsymbol{\mu} = \boldsymbol{\mu}_\ell + \boldsymbol{\mu}_s$ about **B**. Since we wish to evaluate the time average of $E_Z = -\boldsymbol{\mu} \cdot \mathbf{B}$, μ can be considered to be oriented, on the average, along $-\mathbf{J}$ as **J** precesses about **B** (shown in Figure 14.5*b*), even though, instantaneously, $\boldsymbol{\mu}$ is never actually antiparallel to **J**. Thus, we need to calculate $\langle \mu_J \rangle$, the average component of $\boldsymbol{\mu}$ along **J**; E_Z will then be given by

$$E_Z = -\langle \mu_J \rangle B \cos \theta_{JB} \qquad \text{(J)} \tag{13}$$

where θ_{JB} is the constant angle that **J** makes with **B**. This average of μ_J will be given by

$$\langle \mu_J \rangle = \mu_\ell \cos \theta_{LJ} + \mu_s \cos \theta_{SJ} \qquad (\text{C} \cdot \text{m}^2/\text{s}) \tag{14}$$

where θ_{LJ} and θ_{SJ} are the angles that **L** and **S** make with **J**. The cosines of these three angles can be written as

$$\cos \theta_{JB} = \frac{J_z}{J} \qquad \cos \theta_{LJ} = \frac{\mathbf{L} \cdot \mathbf{J}}{LJ} \qquad \cos \theta_{SJ} = \frac{\mathbf{S} \cdot \mathbf{J}}{SJ} \tag{15}$$

These can be evaluated in terms of the quantum numbers for the state. The dot product $\mathbf{L} \cdot \mathbf{J}$ can be evaluated by expanding it as $\mathbf{L} \cdot \mathbf{J} = \mathbf{L} \cdot (\mathbf{L} + \mathbf{S}) = L^2 + \mathbf{L} \cdot \mathbf{S}$. For $\mathbf{L} \cdot \mathbf{S}$, note that $J^2 = (\mathbf{L} + \mathbf{S})^2 = L^2 + S^2 + 2\mathbf{L} \cdot \mathbf{S}$, so that $\mathbf{L} \cdot \mathbf{S}$ can be rewritten as $\frac{1}{2}(J^2 - L^2 - S^2)$. So we have $\mathbf{L} \cdot \mathbf{J} = \frac{1}{2}(L^2 + J^2 - S^2)$. A similar procedure for $\mathbf{S} \cdot \mathbf{J}$ yields $\mathbf{S} \cdot \mathbf{J} = \frac{1}{2}(S^2 + J^2 - L^2)$. Equation 14 now gives $\langle \mu_J \rangle$ in terms of μ_ℓ and μ_s, which are expressed in terms of L and S by using equations 3 and 5 with $g_\ell = 1$ and $g_s = 2$. The result for E_Z, from equation 13, is

$$E_Z = \frac{\mu_0}{2\hbar J}(3J^2 + S^2 - L^2)B\frac{J_z}{J} \qquad \text{(J)} \tag{16}$$

Substituting $m_j\hbar$ for J_z, as in equation 12, and the expressions for J, S, and L in terms of

j, s, and ℓ gives E_Z in the form

$$E_Z = \mu_0 B g_j m_j \qquad \text{(J)} \tag{17}$$

where g_j, known as the **Landé g factor**, is given by

$$g_j = 1 + \frac{j(j+1) + s(s+1) - \ell(\ell+1)}{2j(j+1)} \tag{18}$$

The factor g_j is computed for each level in a multiplet, and is a function j, ℓ, and s for each state; the Zeeman energy can then be calculated for each m_j using equation 17. The total energy for each state is thus $E = E'(n, \ell, j) + E_Z$. Note that for the one-electron atom being discussed here, $S = \frac{1}{2}$ for all states.

EXERCISE 4

Explain why, in the weak-field limit, the average, but not the instantaneous, magnetic moment vector is antiparallel to **J**.

EXERCISE 5

Verify the steps leading to equations 17 and 18.

An important example of a one-electron atom is Na, which has a single optically active electron ($n = 3$) outside closed spherically symmetric electron shells. The first two excited states of the electron along with the ground state are shown in Figure 14.6*a*. The closely spaced yellow D lines, observed for $\mathbf{B} = 0$, are accounted for by transitions to the $^2S_{1/2}$ from the P states. If a weak external field is applied, each state is split, as indicated to the right, so that each D line has several components, separated in energy from the zero-field level by E_Z. The D line spectrum, as it would appear on the photographic plate of a grating spectrometer, is shown schematically in Figure 14.6*b*.

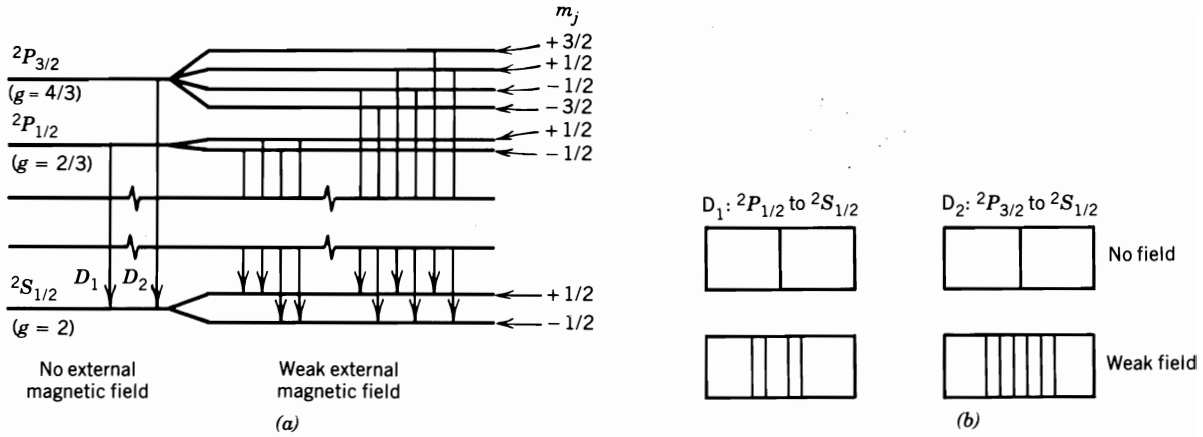

FIGURE 14.6 (*a*) The effect of a weak external magnetic field on three states of Na. (*b*) The effect of a weak magnetic field on the appearance of the Na D-line spectrum on a grating spectrogram.

EXERCISE 6

Verify the assignment of g factors indicated by Figure 14.6*a* to each of the levels. Determine, for each of the Zeeman-split D lines, the shift of the photon energies of the indicated transitions relative to the $B = 0$ values if an electromagnet provides a field of 5 kG. Summarize the results in a rough sketch that indicates schematically how the lines would appear on the photographic plate of a grating spectrograph.

Atoms with Several Optical Electrons

The calculation of the Zeeman patterns can be extended to atoms with more than one optically active electron outside closed shells. The one-electron Hamiltonian of equation 8′ is not adequate to describe the interactions of these electrons with each other: The potential energy is no longer spherically symmetric. The system must be described by a many-electron Hamiltonian that includes the interactions between the optical electrons, and by wave functions that give information about the entire system of optical electrons. The calculation of the electronic states and the Zeeman patterns for these atoms is, in general, quite complex.

For some atoms of intermediate atomic number (for Hg, e.g.), the spin–orbit interaction is weak enough so that its effect may be considered after the stronger effects of the Coulomb interaction between the outer electrons have been taken into account. The effects of a weak external magnetic field are then considered as a perturbation, so that the treatment is quite analogous to that discussed above for a single optical electron. In this scheme, referred to as **Russell–Saunders** (or ***LS***) coupling, the states of the outer electrons are built up by considering the effects of the various interactions in order of their importance. For the simplest case of two outer electrons, the following occurs:

1. These electrons are each assigned quantum numbers n_1, ℓ_1 and n_2, ℓ_2 as if they were individually in states appropriate to the Hamiltonian of equation 8.
2. The relative orientations of the spins are correlated to the spatial motions of the electrons in such a way that states of constant total spin $\mathbf{S}' = \mathbf{S}_1 + \mathbf{S}_2$ are formed, with corresponding quantum number s'. The possibilities for s' are determined from the angular momentum addition rules: s' can have any value from $s_1 + s_2$ down to $|s_1 - s_2|$ in steps of 1. Since $s = \frac{1}{2}$ for electrons, this means, for two electrons, that s' can be 0 or 1. States in which $s' = 0$ are called **singlet** states; $s' = 1$ states are **triplets**. Triplet states are usually lower in energy than singlets.
3. The orbital angular momenta next add to form a total $\mathbf{L}' = \mathbf{L}_1 + \mathbf{L}_2$, so that, in analogy with the spins, the magnitude L' is indexed by the quantum number ℓ' which takes on values from $\ell_1 + \ell_2$ down to $|\ell_1 - \ell_2|$ in steps of 1. The value of ℓ' for a state is designated spectroscopically, as for one electron, by S, P, D, and so on, for $\ell' = 0$, 1, 2, ... States with the lowest value of ℓ' usually have the largest energy.
4. The spin–orbit interaction couples $\mathbf{L}'$ and $\mathbf{S}'$ for a state to form a constant total angular momentum $\mathbf{J}' = \mathbf{L}' + \mathbf{S}'$ as for the single electron. The resulting states of the **multiplet** each have a value of j' that ranges from $\ell' + s'$ down to $|\ell' - s'|$. The spacing between these states of different j' depends on the strength of the spin–orbit interaction; the states with higher j' values have the higher energies.
5. Each state with a given j' corresponds a series of states corresponding to different orientations of $\mathbf{J}$, that is, to different values of $J'_z = m_{j'}\hbar$, where $m_{j'}$ ranges in steps of 1 from $-j'$ to $+j'$. In zero magnetic field, states with different $m_{j'}$ are degenerate; when a weak field is applied, the Zeeman energy shifts are given, as in the one-electron case, by equations 17 and 18 with s', ℓ', j', and $m_{j'}$ substituted for their unprimed counterparts:

$$E_Z = \mu_0 B g_{j'} m_{j'} \quad \text{(J)} \tag{17'}$$

$$g_{j'} = 1 + \frac{j'(j'+1) + s'(s'+1) - \ell'(\ell'+1)}{2j'(j'+1)} \tag{18'}$$

Each state built from an initial configuration $(n_1\ell_1, n_2\ell_2)$ is now characterized by the set of quantum numbers $(s', \ell', j', m_{j'})$. The notation $^{2s'+1}\ell_{j'}$ for each term in a multiplet is the same as for the one-electron case.

This coupling scheme is illustrated schematically in Figure 14.7, for the case of zero external field, for three configurations of the two outer electrons of Hg: the ground state $6s^2$ (i.e., $n_1 = n_2 = 6$, $\ell_1 = \ell_2 = 0$), 6s6p, and 6s7s. Note that for the $6s^2$ configuration, only $s' = 0$ is possible, since the Pauli exclusion principle does not permit the spins $\mathbf{S}_1$ and $\mathbf{S}_2$ to be parallel. The indicated transition $^3S_1 \rightarrow {}^3P_0$ produces the 4046-Å line, which yields a relatively simple Zeeman pattern upon application of an external field. Figure 14.8*a* shows the effect of an external field on these two states. Note that the $^3S_1$ state splits into three, while the $^3P_0$ state is unaffected, thus giving rise to three components in the Zeeman pattern, as indicated in Figure 14.8*b*. The notation employed in this schematic representation of the Zeeman pattern is explained below in connection with selection rules, intensities, and polarizations.

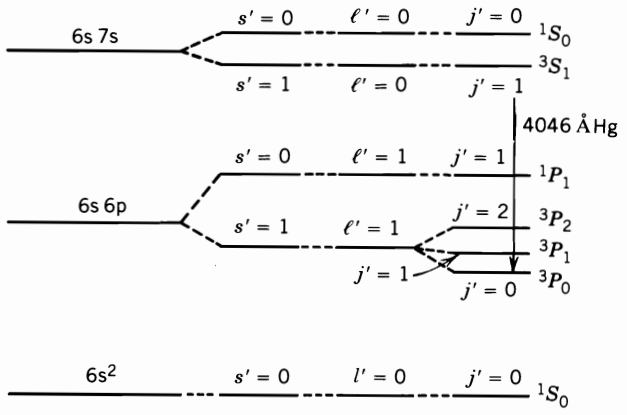

FIGURE 14.7 The *LS* coupling scheme for three states of the two outer electrons of Hg.

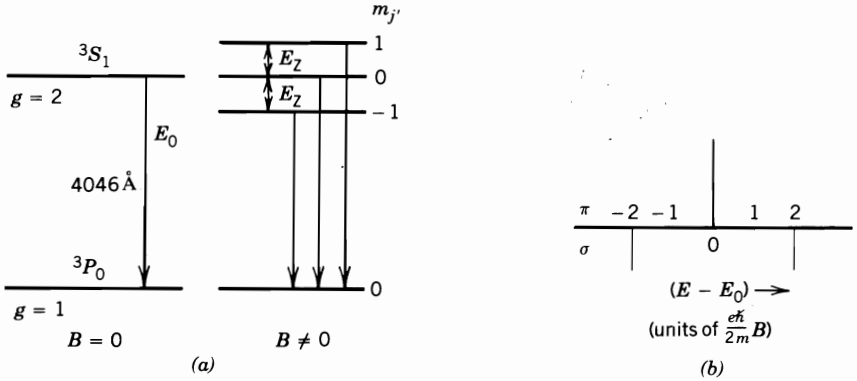

FIGURE 14.8 (*a*) Effect of a magnetic field on the states involved in the emission of the 4046-Å line in Hg. (*b*) The Zeeman pattern for the 4046-Å line in Hg.

EXERCISE 7

Show that the Zeeman components of the 4046 Å in Hg are separated in energy by $E_Z = e\hbar B/m$.

Selection Rules, Intensities, and Polarizations

The formalism of quantum mechanics not only allows us to predict the wavelengths of the Zeeman components of a spectral line, but also can relate the appearance of the pattern to the nature of the states involved in the various transitions.

The intensity with which a given wavelength is emitted in an atomic transition is proportional to the probability with which that transition occurs. This can be calculated by computing the matrix element of the electric dipole moment $\mathbf{P} \equiv \Sigma_i e\mathbf{r}_i$, where $\mathbf{r}_i$ is the position of the ith optically active electron in the atom, by evaluating the expression

$$\mathbf{P}_{\text{fi}} = \int \psi_{\text{f}}^* \mathbf{P} \psi_{\text{i}}\, dV \qquad (\text{C} \cdot \text{m}) \tag{19}$$

where ψ_{i} and ψ_{f} are the initial and final states of the atom. The relative intensities of the various components of a Zeeman pattern are then each approximately proportional to P_{fi}^2. Calculated for the set of transitions corresponding to any pair of states ${}^{2s'+1}\ell'_{j'}$ (e.g., to the D_1 line shown in Figure 14.6), the relative intensities depend only on the initial and final values of j' and $m_{j'}$ for each individual component, independent of the kind of atom to which the LS coupling scheme has been applied.

Selection rules arise from the observation that certain of the dipole matrix elements are almost zero, so that transitions between certain states are *forbidden*, that is, make almost no contribution to the observed spectral pattern. If there is no external magnetic field, the "allowed" ($P_{\text{fi}} \neq 0$) transitions must, for the LS coupling scheme, satisfy the conditions

$$\begin{aligned} &\Delta s' = 0 \\ &\Delta \ell' = 0,\ \pm 1 \\ &\Delta j' = 0,\ \pm 1 \quad (\text{but } j' = 0 \rightarrow j' = 0 \text{ is forbidden}) \end{aligned} \tag{20}$$

for the changes in these quantum numbers during a transition. When an external magnetic field is applied, the number of observable transitions increases, but these are subject to the additional selection rule

$$\Delta m_{j'} = 0,\ \pm 1 \quad (\text{but } m_{j'} = 0 \rightarrow m_{j'} = 0 \text{ is forbidden if } \Delta j' = 0) \tag{21}$$

EXERCISE 8

Verify that all of the transitions indicated in Figure 14.6 are consistent with the selection rules stated above.

Evaluation of P_{fi}^2 for each pair of initial and final states that satisfy the selection rules gives expressions for the total relative radiated intensity I of each component of the Zeeman pattern, in arbitrary units (reference 3):

For $j' \rightarrow j' - 1$ transitions

$$\begin{aligned} m_{j'} \rightarrow m_{j'} \pm 1 \qquad & I = \tfrac{1}{2}a(j' \mp m_{j'} - 1)(j' \mp m_{j'}) \\ m_{j'} \rightarrow m_{j'} \qquad & I = a(j' + m_{j'})(j' - m_{j'}) \end{aligned} \tag{22}$$

For $j' \rightarrow j'$ transitions

$$m_{j'} \rightarrow m_{j'} \pm 1 \qquad I = b(j' \mp m_{j'})(j' \pm m_{j'} + 1)$$
$$m_{j'} \rightarrow m_{j'} \qquad I = bm_{j'}^2$$

where a and b are constants. The expressions for the $j' \rightarrow j' + 1$ transitions may be added by considering the reverse of the $j' \rightarrow j' - 1$ transitions and noting that forward and reverse intensities are the same ($P_{\text{fi}}^2 = P_{\text{if}}^2$).

Experimental observations of the Zeeman effect seldom measure the total intensities directly, since detection systems generally measure light emerging from the atom in a narrow range of directions. It is important to note that the radiation emitted by the transitions considered above is anisotropic: The intensity as well as the polarization of the light in each component (for each value of $\Delta m_{j'}$) depends on the direction of emission relative to **B** and on $\Delta m_{j'}$ for the associated transition. Figure 14.9 is a top view that illustrates the polarization of light emitted parallel to **B** (longitudinally) and perpendicular to **B** (transversely).

For the *transverse* observation, the emitted radiation is *linearly* polarized: for transitions in which $\Delta m_{j'} = 0$, called the π components, the electric field ϵ of the radiation is parallel to the applied field **B**; for the $\Delta m_{j'} = \pm 1$ transitions, or the σ components, ϵ is perpendicular to **B** and thus oscillates along a direction perpendicular to the plane of the paper, as indicated by the symbol in the figure.

For *longitudinal* observations, the σ components are *circularly* polarized, and the π components do not appear. Since all components of a Zeeman pattern are visible when viewed transversely, this is the experimental arrangement most often used. The relative intensities for the individual components in the transverse direction are given by

For $j' \rightarrow j' - 1$ transitions

$$m_{j'} \rightarrow m_{j'} \pm 1 \qquad I = a'(j' \mp m_{j'} - 1)(j' \mp m_{j'})$$
$$m_{j'} \rightarrow m_{j'} \qquad I = 4a'(j' + m_{j'})(j' - m_{j'}) \tag{23}$$

For $j' \rightarrow j'$ transitions

$$m_{j'} \rightarrow m_{j'} \pm 1 \qquad I = b'(j' \pm m_{j'} + 1)(j' \mp m_{j'})$$
$$m_{j'} \rightarrow m_{j'} \qquad I = 4b'm_{j'}^2$$

where a' and b' are constants and the units for I are again arbitrary. For a given Zeeman pattern, the total intensity of the emitted radiation from all allowed transitions is isotropic and, on the average, has no net polarization.

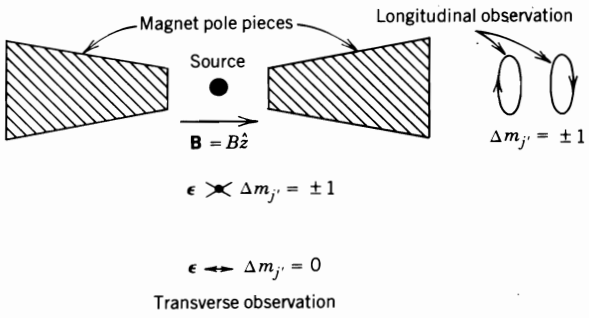

FIGURE 14.9 Polarization of the components of a Zeeman pattern.

Figure 14.8*b* illustrates the way in which the Zeeman pattern is conventionally represented for a transverse observation. The horizontal axis represents the transition energy, relative to that of the zero-field transition. The π and σ components are represented above and below this axis, respectively, by vertical lines with heights proportional to the intensities.

The observed polarization states are sometimes explained by considering the radiation produced by the oscillating dipole associated with the classical electron orbit for the various possible atomic orientations, as in Figure 14.1*b*. This is little more than a mnemonic device, since the nature of the radiation must be associated with the motion of the charge *during the transition* that produces it. Thus, the polarization can be understood by evaluating the time-dependent expectation value of the dipole moment $\mathbf{P}(t)$ during the transition, when the states can be expressed as a mixture of initial and final states ψ_i and ψ_f. $\mathbf{P}(t)$ can be expressed in terms of the quantity $\mathbf{P}_{fi}$ of equation 19:

$$\mathbf{P}(t) \propto \mathrm{Re}[\mathbf{P}_{fi} \exp(i\omega t)] \qquad (\mathrm{C} \cdot \mathrm{m}) \tag{24}$$

where $\omega \equiv (E_f - E_i)/\hbar$ is the frequency of the photon emitted in the transition between the two states of energy E_i and E_f. For π transitions, $\mathbf{P}$ oscillates along the z direction, so that radiation polarized along $\hat{z}$ would be viewed transversely, but no radiation is emitted longitudinally, along the dipole axis. For σ transitions, $\mathbf{P}$ rotates in the xy plane, producing circularly polarized light viewed along $\hat{z}$; when viewed transversely $\mathbf{P}$ appears as a linear dipole, perpendicular to $\hat{z}$, and so produces an $\boldsymbol{\epsilon}$ perpendicular to the magnetic field.

EXERCISE 9

Verify that the transverse intensities for the Hg 4046-Å line that are indicated in Figure 14.8*b* correctly correspond to the transitions of Figure 14.8*a*.

EXERCISE 10

Make a sketch, similar to Figure 14.8, for the Hg 5461-Å line, which is produced by a $^3S_1 \rightarrow {}^3P_2$ transition. Indicate, for the allowed transitions, the relative transverse intensities and the energy spacings relative to the zero-field energy.

EXPERIMENT

Listed in Table 14.1 are a few transitions suitable for Zeeman effect observations in Hg, Na, and He—three atoms for which the above discussion of *LS* coupling is appropriate. For the Hg investigations, a sample enriched with ^{198}Hg (available commercially) should be used since its nucleus has zero spin; thus, the complications of the hyperfine structure associated with the magnetic moment of the nucleus are avoided.

The high resolution required for the observation of the Zeeman splittings may be obtained by use of either an Ebert-mount spectrograph or a Fabry–Perot interferometer; recording of the spectra may be done either photographically or with a phototube. The Ebert-mount spectrograph is described in Appendix D; below we briefly describe the operation of the Fabry–Perot device and an experiment that utilizes it with the phototube.

TABLE 14.1 SOME TRANSITIONS SUITABLE FOR ZEEMAN EFFECT OBSERVATIONS

Atom	*Color*	*Wavelength* (Å)	*Initial Configuration*	*Final Configuration*
Hg	Violet	4046	6s 7s $^3S_1$	6s 6p $^3P_0$
	Yellow	5791	6s 6d $^1D_2$	6s 6p $^1P_1$
	Green	5461	6s 7s $^3S_1$	6s 6p $^3P_2$
	Violet	4358	6s 7s $^3S_1$	6s 6p $^3P_1$
	Yellow	5770	6s 6d $^3D_2$	6s 6p $^1P_1$
Na	Yellow	5896	3p $^2P_{1/2}$	3s $^2S_{1/2}$
	Yellow	5890	3p $^2P_{3/2}$	3s $^2S_{1/2}$
He	Blue	4471	4d $^3D_3$	2p $^3P_2$
	Green	5016	3p $^1P_1$	2s $^1S_0$
	Yellow	5875	3d $^3D_3$	2p $^3P_2$

The Fabry–Perot Etalon

Consider a ray of monochromatic light, of vacuum wavelength λ_0, incident on an etalon consisting of a pair of parallel glass plates separated by a gap of width d filled with a medium with index of refraction n_f, as illustrated in Figure 14.10. The inner surfaces of the plates are partially mirrored so that, if the angle of incidence θ is small, the ray is multiply reflected. The optical path for each of the rays emerging at the right is different, so that beams will exhibit interference. The phase difference between adjacent emerging rays can be calculated by considering $\delta\ell$, the difference in path lengths for the rays emerging at B and D. Relative to the ray emerging at B, the ray reflected at B has an additional path length, measured from B to the wave front at D', of $\delta\ell = BC + CD' = 2d\cos\theta$. If we neglect the relatively small additional phase changes due to the metallic film, the difference in phase, $\delta\phi$, for these two rays is

$$\delta\phi = 2\pi\frac{\delta\ell}{\lambda} = 4\pi n_f \cos\theta\,\frac{d}{\lambda_0} \qquad \text{(rad)} \tag{25}$$

where $\lambda = \lambda_0/n_f$ is the wavelength in the medium between the plates. The intensity I_t of the radiation transmitted through the Fabry–Perot will be a maximum if the beams interfere

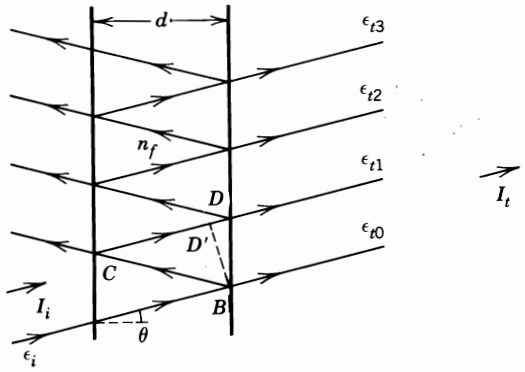

FIGURE 14.10 Multiple reflections of a beam between the plates of a Fabry–Perot etalon.

constructively, that is, if, for some integer m,

$$\delta\phi = 2\pi m \qquad \text{(rad)} \tag{26}$$

EXERCISE 11

Verify trigonometrically the relationship $\delta\ell = 2d\cos\theta$, which leads to the expression for $\delta\phi$ of equation 25.

The amplitude of the transmitted electric field ϵ_t^0 can be found in terms of the incident amplitude ϵ_i^0 by superposing, with appropriate phase factors, the time-dependent field strengths of the transmitted beams. As in Figure 14.10, the time-varying strength of the electric field ϵ_{tk} of the kth transmitted beam can be written as $\epsilon_{tk}^0 \exp(i\omega t)$, where $k = 0$ corresponds to the first transmitted beam, which has not been reflected. The field transmission and reflection coefficients for the inner surfaces of the plates, t and r, can then be used to write $\epsilon_{tk}^0 = t^2 r^{2k} \epsilon_i^0$. The phase of the kth beam lags behind that of the $k = 0$ beam by an amount $k\,\delta\phi$. The field strength ϵ_t is then expressed as

$$\begin{aligned}\epsilon_t &\simeq \sum_{k=0}^{\infty} \epsilon_{tk}^0 \exp[i(\omega t - k\,\delta\phi)] \\ &= \left[\sum_{k=0}^{\infty} (t^2 r^{2k}) \exp(-ik\,\delta\phi)\right] \epsilon_i^0 \exp(i\omega t) \qquad \text{(N/C)}\end{aligned} \tag{27}$$

where the number of reflections has been assumed so large that ϵ_t may be approximated by extending the series to an infinite number of terms. Evaluating this geometrical series yields

$$\epsilon_t = \left[\frac{T}{1 - R\exp(-i\,\delta\phi)}\right] \epsilon_i^0 \exp(i\omega t) \qquad \text{(N/C)} \tag{28}$$

where $T = t^2$ is the transmittance and $R = r^2$ the reflectance of the metal film. Since the intensity of the emerging beam is proportional to $\epsilon_t \epsilon_t^*$, equation 28 gives the ratio of transmitted and incident intensities as

$$\frac{I_t}{I_i} = \left(\frac{T}{1-R}\right)^2 \frac{1}{1 + F\sin^2(\delta\phi/2)} \tag{29}$$

where the abbreviation $F \equiv 4R/(1-R)^2$ and the identity $\cos\delta\phi = 1 - 2\sin^2(\delta\phi/2)$ have been used. This ratio is plotted in Figure 14.11*a* as a function of the phase difference $\delta\phi$ for

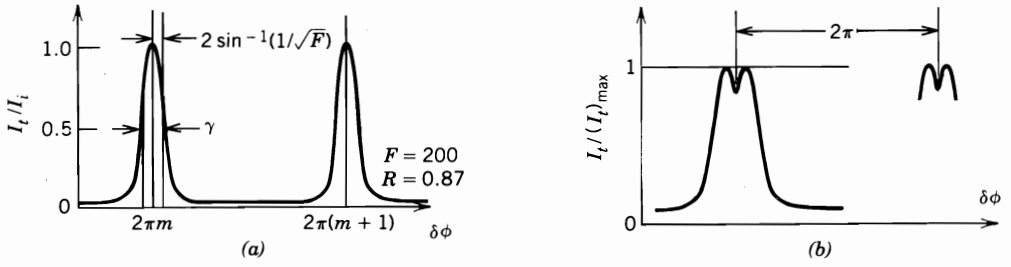

FIGURE 14.11 (*a*) The ratio of transmitted and incident intensities for a Fabry–Perot etalon with $R = .87$. (*b*) Intensity pattern from a Fabry–Perot for two barely resolved peaks.

a reflectivity of $R = 0.87$, assuming that the reflecting film absorbs no energy (i.e., that $T + R = 1$). Note, as mentioned above, that the peaks in the transmission occur for $\delta\phi = 2\pi m$.

Two ways in which the etalon can be used to measure wavelength are illustrated in Figure 14.12. If an extended source is configured with the etalon and two converging lenses, as in Figure 14.12*a*, rays enter the first plate of the Fabry–Perot with a range of incident angles θ. Each value of θ corresponds to a value of $\delta\phi$ given by equation 25 and to a radial position on a screen or photographic plate to which rays with this value of θ are focused; a series of bright rings are formed with radii corresponding to values of θ for which $\delta\phi = 2\pi m$. Measurements of these radii may then be used along with equations 25 and 26 to calculate the wavelength differences between the spectral components of the light from the source. As is discussed in reference 8, the wavelength separation for two adjacent fringes (corresponding to the same order m) with diameters D and D' is given by

$$\Delta\lambda = \lambda(D^2 - D'^2)/8f^2 \qquad \text{(m)} \tag{30}$$

where f is the focal length of the lens between the screen and the etalon.

A second method for determining spectral splittings, discussed further below in connection with the Zeeman effect measurements, is called central spot scanning, illustrated by Figure 14.12*b*. In this technique, the index of refraction n_f or the etalon spacing d is varied, thus changing $\delta\phi$. Peaks in I_t are observed for the light allowed through the pinhole, for which $\theta = 0$. From the curve of I_t versus n_f (or d), one can deduce the separations in λ for the various components of the incident beam.

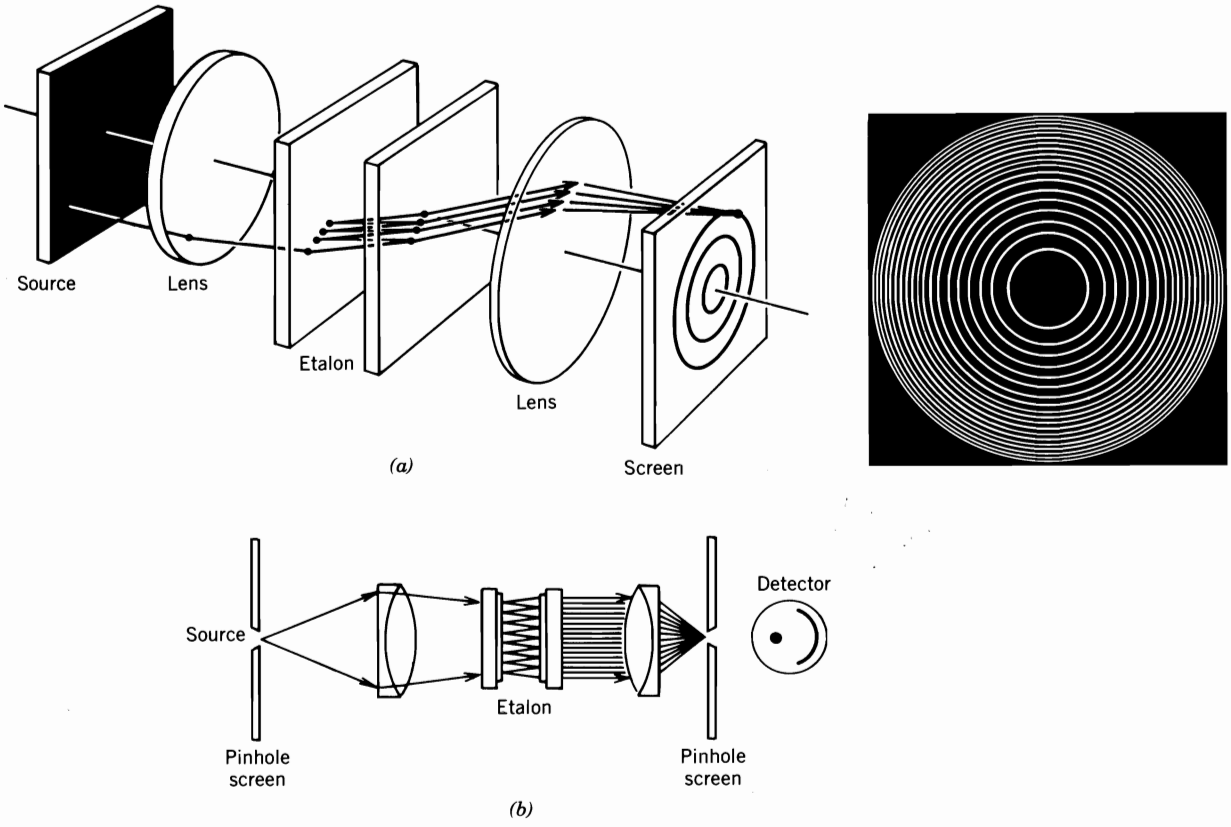

FIGURE 14.12 (*a*) Ring pattern produced by a Fabry–Perot with an extended source. (*b*) Central spot scanning with a Fabry–Perot.

Two parameters that determine the suitability of the Fabry–Perot for a particular set of measurements are the **free spectral range** $\Delta\lambda_{0f}$ and the **finesse** F_0. The free spectral range is that difference in wavelength between two spectral components of the source whose intensity maxima just overlap, that is, $\delta\phi(\lambda_0) - \delta\phi(\lambda_0 + \Delta\lambda_{0f}) = 2\pi$. Using equation 25 for $\delta\phi$ gives $\Delta\lambda_{0f}$ for $\theta = 0$:

$$\Delta\lambda_{0f} \simeq \frac{\lambda_0^2}{2n_f d} \qquad \text{(m)} \tag{31}$$

EXERCISE 12

Verify that this expression for $\Delta\lambda_{0f}$ is nearly exact for visible wavelengths and an etalon having $d = 0.500$ cm and $n_f = 1$. What is $\Delta\lambda_{0f}$ in this case if $\lambda_0 \simeq 4046$ Å?

The finesse F_0 is the ratio of the separation, in $\delta\phi$, of two adjacent maxima in Figure 14.11*a* to the full width at half-maximum (FWHM) of the peaks, labeled γ. F_0 can be related to the reflectivity of the etalon surface by noting that equation 29 implies that, for large values of the parameter F (defined below, equation 29), I_t falls to one half its maximum value when $\delta\phi$ deviates by $2/F^{1/2}$ radians from $2\pi m$, its value at the mth peak. The full width γ is just double this amount, so $\gamma = 4/F^{1/2}$. Since two adjacent peaks are separated by a phase difference of 2π, $F_0 \equiv 2\pi/\gamma = \pi F^{1/2}/2$. Substituting the definition of F equation (29) gives F_0 in terms of R:

$$F_0 = \frac{\pi\sqrt{R}}{1 - R} \tag{32}$$

EXERCISE 13

Verify that I_t falls to half of its maximum value when $\delta\phi$ deviates from a peak value by $2/F^{1/2}$ radians. What approximation must be made to obtain this result?

We will say that two wavelengths λ_1 and $\lambda_2 \equiv \lambda_1 + \Delta\lambda_0$ are resolvable with the etalon if the phase differences $\delta\phi_1$ and $\delta\phi_2$ to which they correspond (for fixed values of n_f, θ, and d near a transmission peak) are different by at least the FWHM, γ, of the I_t/I_i versus $\delta\phi$ curve: $\delta\phi_1 - \delta\phi_2 \gtrsim 2\pi/F_0$ for resolution of the two wavelength components. Figure 14.11*b* illustrates the intensity pattern due to two closely spaced wavelength components whose peaks are just barely resolved. To express the above resolution criterion directly in terms of wavelength separation, an approximation for $\delta\phi_1 - \delta\phi_2$ in terms of $\Delta\lambda_0$ may be obtained by differentiating equation 25 with respect to λ_0, giving us $\delta\phi_1 - \delta\phi_2 \simeq \delta\phi(\lambda_0)(\Delta\lambda_0/\lambda_0)$, where $\lambda_0 \simeq \lambda_1 \simeq \lambda_2$. Since $\delta\phi(\lambda_0) \simeq 2\pi m$ near a peak, this means that two wavelengths may be resolved if $\Delta\lambda_0 \gtrsim \lambda_0/mF_0$. The ratio of λ_0 to the minimum resolvable wavelength difference, $(\Delta\lambda_0)_{min}$, is the **chromatic resolution** R_0 and is given by

$$R_0 \equiv \frac{\lambda_0}{(\Delta\lambda_0)_{min}} = mF_0 = \frac{\pi m\sqrt{R}}{1 - R} \tag{33}$$

EXERCISE 14

For the situation described in Exercise 12, estimate the chromatic resolution of an etalon with surfaces that are 87 percent reflecting. Is this resolution sufficient for the study of the Zeeman pattern of, for example, the 4046-Å line of Hg using the magnetic fields available

to you in your laboratory? What other factors will determine your ability to resolve the individual components of the Zeeman pattern?

Zeeman Effect Measurements

Figure 14.13*a* is a block diagram of the apparatus that can be used for the transverse observation of the Zeeman effect through the use of the central spot scanning technique described above. Light from the source, located between the magnet pole pieces, passes through converging lens 1 (and, optionally, through a polaroid sheet) so that it is incident on the Fabry–Perot etalon as a parallel (linearly polarized) beam at normal incidence. The etalon is located in a vacuum chamber, which can be evacuated and refilled with an adjustable leak (e.g., with a needle valve control); the index of refraction n_f can thus be varied by varying the pressure in the chamber. Lens 2 focuses light exiting the etalon onto the slit of a constant-deviation prism spectrometer (discussed in reference 6, Section 5.5); the prism can be rotated so that light from the spectral line under investigation can be viewed at the eyepiece. The data are taken by replacing the eyepiece with a pinhole so that

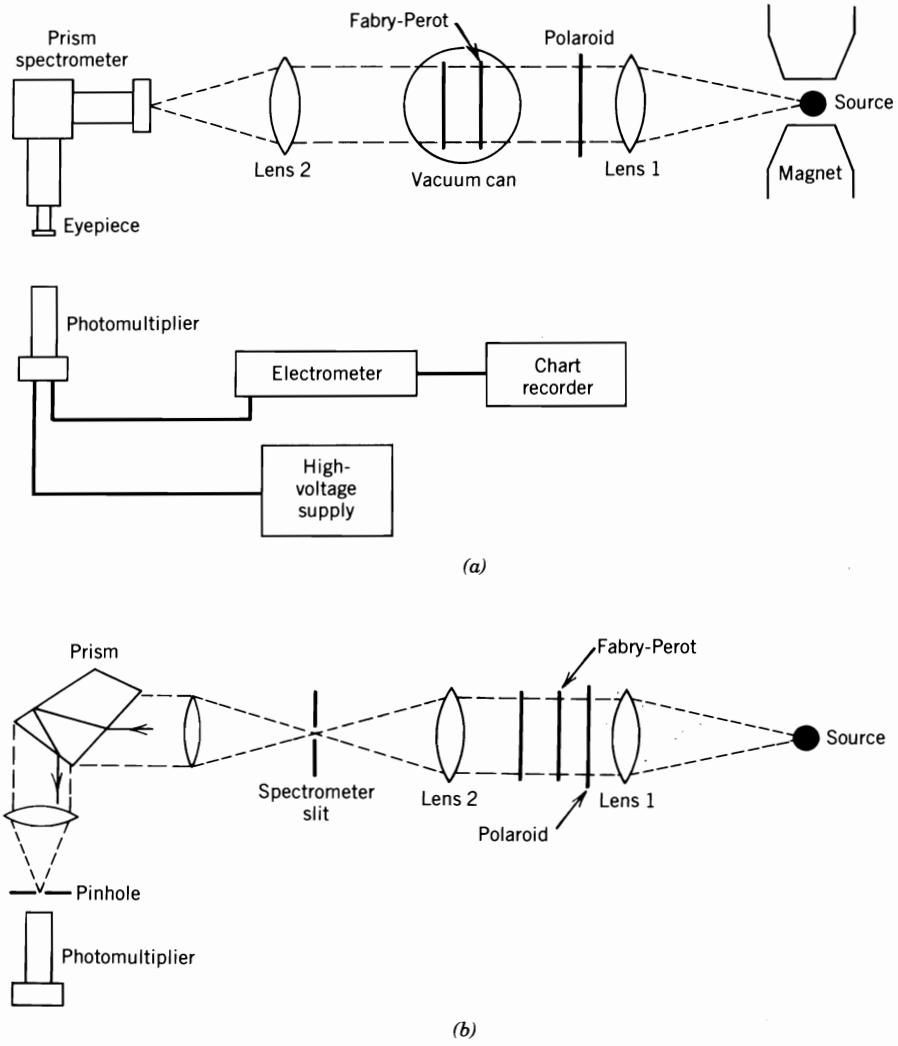

FIGURE 14.13 (*a*) Apparatus for the transverse observation of the Zeeman effect. (*b*) Optical arrangement for the observation of the Zeeman effect.

light from the center of the Fabry–Perot pattern enters the photomultiplier tube. The photocurrent is detected with an electrometer, the output of which is connected to a chart recorder. Some further details of the optical system for this mode of operation are included in Figure 14.13*b*.

With the Fabry–Perot "crossed" with the prism spectrometer in the fashion described above, scanning of the Zeeman pattern is accomplished by slow readmission of gas into the evacuated vacuum chamber, which results in an n_f that varies in an approximately linear way with time. If the output of the phototube is then recorded as a function of time, the result will be a scaled version of the intensity versus n_f curve. For each wavelength component, the phase difference $\delta\phi$ is, according to equation 25, proportional to n_f, so that for a single wavelength (e.g., for a spectral line observed with $B = 0$), a portion of the I_t versus n_f curve derived from a pressure scan would appear as in Figure 14.14*a*; for two closely spaced wavelengths, the scan would produce a double-peak pattern, shown in Figure 14.14*b* for the case of unequal intensities. The splitting $\lambda_2 - \lambda_1$ can be estimated in terms of n_{f1}, n_{f2}, the free spectral range $\Delta\lambda_{0f}$, and Δn_{f0}, the change in n_f between successive orders:

$$\frac{\lambda_2 - \lambda_1}{\Delta\lambda_{0f}} \simeq \frac{n_{f2} - n_{f1}}{\Delta n_{f0}} \tag{34}$$

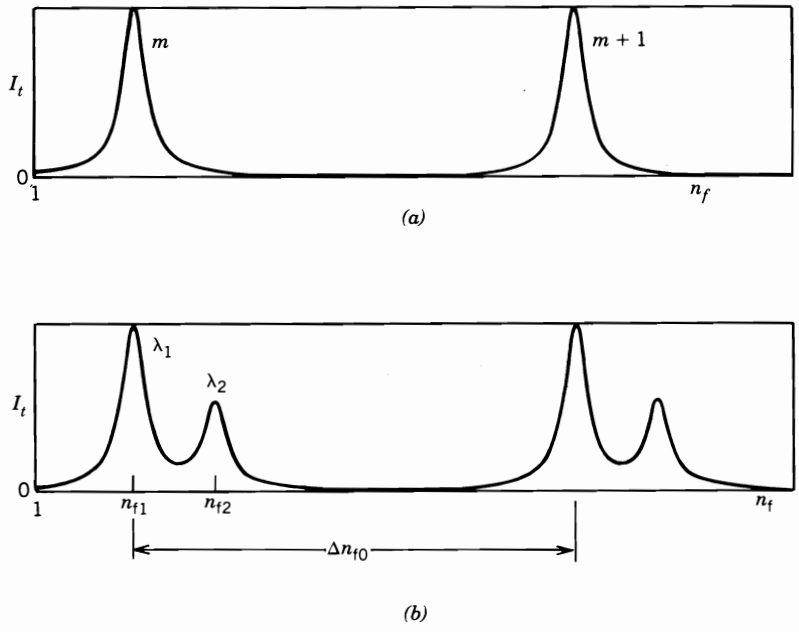

FIGURE 14.14 (*a*) I_t versus n_f curve derived from a pressure scan. (*b*) Appearance of the I_t versus n_f curve in the case of two closely spaced peaks.

EXERCISE 15

For the wavelength and etalon in Exercise 12, estimate the number of intensity peaks that would be seen in a scan from zero pressure up to atmosphere, if $n_f \simeq 1.000277$ at 1 atm pressure.

With the Fabry–Perot and its vacuum can out of the optical path, collimate the light from the source with lens 1 so that it does not spread along the path. Use lens 2 to focus

the light on the spectrometer slit. With the eyepiece in place, adjust the spectrometer and lens 2 to obtain the brighest spectral line images. Place the etalon, with its vacuum can, in the optical path and adjust it so that the ring pattern is centered in the eyepiece; the light reflected from the etalon should be directed back toward the source. Adjust the pressure for a peak in the intensity of the light entering the spectrometer and replace the eyepiece with the pinhole and phototube assembly. Maximum signal can be obtained by adjustments of the focus and the prism orientation.

The strength of the magnetic field should be measured for each set of observations. To eliminate error due to hysteresis in the magnet iron, the field measurements should be taken after the scan and before changing the magnet current.

For the spectral line(s) selected, predict the Zeeman patterns and produce pressure scans at a few different values of B. The central component may be filtered out with a polarizer to facilitate measurements of the splittings. As is suggested above, these splittings may be estimated as fractions of the free spectral range.

EXERCISE 16

The superposition of intensities from two closely spaced peaks will cause the measured separation in wavelength to be different from its actual value. Will your measurements then yield overestimates or underestimates of the splittings? How would you attempt to correct for this error? Note in this connection that the best data are obtained for splittings that amount to about one half of the free spectral range.

EXERCISE 17

Investigate the linearity of the splittings as functions of the field and derive, for each observed pattern, a value of μ_0 for comparison with its accepted value. Repeat enough of the measurements to derive an estimate of the associated uncertainties. Do your observations support the theory of LS coupling? If you can estimate your relative intensities, are they what you expect?

Summary

In atoms of intermediate atomic number for which the structure of the optical electrons is adequately described by the Russell–Saunders coupling scheme, the states (wave functions) for these electrons may be described by the quantum numbers s', ℓ', j', and $m_{j'}$. The energy of these states may be expressed as $E = E'(n, s', \ell', j') + E_Z$, where E_Z is the Zeeman energy, given by

$$E_Z = \mu_0 B g_{j'} m_{j'} \qquad \text{(J)} \tag{17'}$$

where the Landé g factor is

$$g_{j'} = 1 + \frac{j'(j'+1) + s'(s'+1) - \ell'(\ell'+1)}{2j'(j'+1)} \tag{18'}$$

The energy levels E' are illustrated schematically for a few multiplets of Hg in Figure 14.7, and Figure 14.8 illustrates the effect of a magnetic field on these levels, that is, the Zeeman effect. For spectral lines resulting form the transitions between pairs of states in different multiplets, calculations of the dipole matrix elements leads to selection rules, intensities, and polarizations for the radiation emitted in various directions.

The Zeeman effect may be investigated quantitatively by measuring the splitting, produced by an externally applied magnetic field, of the spectral lines corresponding to transitions between states of a multiplet. The high resolution required can be obtained by use of either an Ebert-mount spectrograph or by a Fabry–Perot interferometer. The central spot scanning technique for the Fabry–Perot etalon, illustrated in Figure 14.13, produces intensity peaks, as in Figure 14.14, from which measurements of the Bohr magneton may be derived.

COMPUTER-ASSISTED EXPERIMENTATION (OPTIONAL)

Prerequisite

Experiment 6, Introduction to Computer-Assisted Experimentation.

Introduction

The relatively simple method of acquiring and analyzing the Zeeman effect data suggested above depends for its success on the linearity of the relationships (a) between n_f (the index of refraction of the air between the reflecting surfaces of the interferometer) and p (the pressure), and (b) between p and the time elapsed since beginning the readmission of air to the can, which is measured on the time axis of the chart recorder. The linearity between pressure and time may be improved by using a needle valve to impose a very low flow rate for the air; this also minimizes effects due to local temperature changes and turbulence during the pressure scan. The magnitude of the problem posed by the nonlinearity of n_f versus p can be assessed by examining the quantity $\partial n_f/\partial p$, which is given by reference 7 for a constant temperature of $T = 15\ ^\circ\text{C}$ as

$$\left(\frac{\partial n_f}{\partial p}\right)_{T=15\ ^\circ\text{C}} = (n_f^0 - 1)(1.3149 \times 10^{-3} + 1.626 \times 10^{-9}p) \tag{35}$$

where p is in torr and n_f^0 is the index for air at $p = 760$ torr and $T = 15\ ^\circ\text{C}$. The effect of the nonlinearity given by this relationship depends on the range of pressures used in the scan, but is small for most cases of practical interest.

These nonlinearities can be effectively compensated for by a computer interface that utilizes software to linearize these data. Additionally, the computer affords a convenient method for averaging data (from the same scan or from different scans) in the event that low signal levels make this appropriate.

EXERCISE 18

Using equation 35, derive an expression for the index of refraction as a function of p at 15 °C. For the pressure range required to scan one free spectral range at optical wavelengths with your etalon, estimate the percentage by which the corresponding actual change in n_f deviates from the change calculated under the assumption of complete linearity.

Experiment

The configuration we suggest for computer-assisted data acquisition from central spot scans is shown in Figure 14.15. The output of the pressure transducer is an analog voltage that is linearly related to the pressure within the vacuum can; this signal is input, via a conditioning circuit (if required), to one of two input channels of the ADC that are to be polled for data by the software. The output of the electrometer is fed to a second channel via another conditioning circuit.

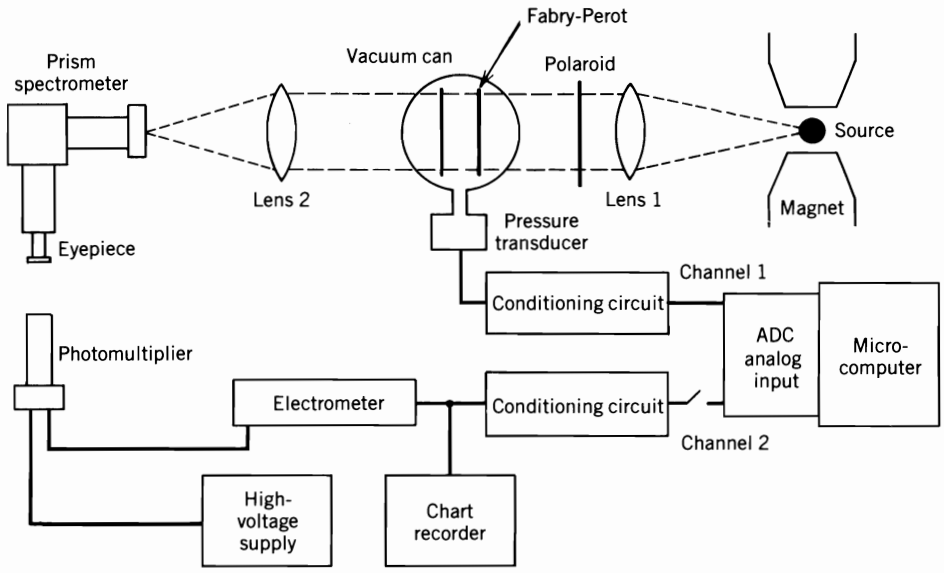

FIGURE 14.15 Configuration for computer-assisted data acquisition.

If the output of the pressure transducer matches the ADC input range, then no conditioning circuit is required. If conditioning is required, a modification of the circuit shown in the upper half of Figure 6.5 (consisting of op-amps 1 and 2) can be used to provide the appropriate gain and offset. The transducer output ground can be directly connected to pin 3 of op-amp 1 and resistors R_3 and R_4 can be eliminated. R_2 and V_{off} should be adjusted so that the full range of the ADC input is utilized for maximum precision.

The conditioning circuit for the electrometer output may be of the same design as that for the transducer, but since the input signal range during the scan will be determined by the light intensity and the electrometer scale setting, it is a good idea to adjust the conditioning gain and offset by setting up and observing some scans on the chart recorder before switching the output of the conditioning circuit into channel 2 of the ADC.

Measurements and Software Both pressure and intensity data may be taken "on the fly" by polling channels 1 and 2 of the ADC input periodically as air is slowly readmitted to the vacuum can containing the Fabry–Perot. Write a program to take the data and to produce values of n_f and intensity at intervals during a scan; produce a graph of these results. You may wish to develop averaging schemes and/or attempt to process this data to produce values of the Zeeman splittings directly.